Preparing the Chemical Laptop for Field Analysis

Eugene Lynch
Mentors: Peter Willis, Amanda Stockton
9-26-2013

Abstract

The Chemical Laptop, co-engineered with Los Gatos Research and HJ Science & Technology, is a portable, miniaturized instrument designed to detect molecular signatures of life in liquid samples. Operated by a tablet computer, it uses microcapillary electrophoresis (µCE) coupled with laser-induced fluorescence detection (LIFD) to analyze labeled samples pneumatically prepared and transported on a multilayer microfluidic chip. Several modifications were made to the instrument's software and hardware to prepare for a completely automated end-to-end field analysis. Existing software was revised to reduce the complexity of spectral data and optimize automated sample processing cycles. New software was written, allowing for automated, on-chip colorimetric determination and adjustment of sample pH. A variety of fabrication methods, materials, and post-fabrication procedures were explored to develop a lightweight, air-tight, pneumatic manifold resistant to deformation under high pressure. Different micropumps were tested to supply sufficent pressure to this manifold. New hardware was developed to make the instrument field-deployable. A simple mounting system was installed to position a USB microscope above the microfluidic chip, allowing for colorimetric pH control and remote observation. Miniature, modular, refillable cartridges were prototyped to dispense all necessary reagents required for the analysis of numerous compound classes by a simple clamping and switching mechanism.

I. Background

The Willis Lab at Jet Propulsion Laboratory focuses on the developent of microdevices capable of automated, in-situ chemical analyses for use in planetary exploration missions as well as on Earth. Our latest prototype instrument, co-engineered with small business partners Los Gatos Research and HJ Science & Technology, performs such analyses on molecular signatures of life (amino acids, carboxylic acid derivatives, thiols, etc.) through a coupling of microchip capillary electrophoresis (µCE) with laser-induced fluorescence detection (LIFD). In the last decade, µCE-LIFD has gained popularity as an analytical tool for chemical and biochemical analysis.[1,2,3,4] The principle of µCE is identical to typical capillary electrophoresis (CE). A high voltage applied across an electrophoretic channel separates an injected liquid sample mixture into component analytes grouped by their respective mass to charge ratios. Detection is achieved by laser-excitation and fluorescence detection of derivatized samples. µCE, however, uses a separation column that is only 100 µm wide, and 20 cm long. This extreme miniaturization, achieved through innovative microfabrication procedures, allows for high separation efficiency (<100 µL) rapid analyses (<5 min), and ready integration into miniaturized detection formats. The coupling of LIF detecton to µCE allows for parts-per-trillion (ppt) levels of sensitivity. Furthermore, the technology, relying only on electric potential and capillary action as driving forces, has shown success in microgravity environments.[5]

The Chemical Laptop's novelty stems from its ability to integrate automated, microfluidic sample processing (sample derivatization, mixing, dilution, pH adjustment) with the µCE chip. Since µCE-LIFD requires sample derivatization and reagent mixing, this on-chip, multifunctional processing capability is absolutely necessary for truly automated in-situ analyses. The instrument can be adapted to several different chemical processing operations through simple software programming. This enables the user to mix up to 16 different liquid reagents in any proportion before exporting for analysis.

II. Instrumentation

The Chemical Laptop (Fig.1) combines all the components necessary for automated µCE-LIFD analysis into a compact, low-power instrument measuring 38.1 x 11.6 x 25.4 cm with a power consumption maximum of 10W during normal operation.

To achieve automation of µCE-LIF analytical processes, a multilayer glass-PDMS hybrid microfluidic device is utilized (Fig.2). The device consists of four layers: a pneumatic layer etched in glass, a flexible elastomeric membrane layer, an etched fluidic layer, and an etched µCE channel layer. The first layer of the chip, the "pneumatic layer," contains a two-dimensional array of valves and plumbing to off-chip vacuum / pressure inputs. The fluidic layer contains a two dimensional network of fluidic channels; and the membrane is sandwiched between the featured side of this layer and the pneumatic layer. When a vacuum input is applied to the pneumatic layer at a position opposite a discontinuity in the fluidic layer, the membrane deflects into the pneumatic layer, enabling fluidic flow over the discontinuity (Fig. 3). Actuation

of two or more valves in series can form a peristaltic pump, and valves are actuated in a pre-programmed series to drive fluidic movement through interconnecting channels on the chip. Multipurpose reservoirs on the outer rim of the array are used for sample import/export, and for storage of dyes (to label functional groups of interest), buffers (to regulate pH), standards (for calibration and comparison of experimental results), and treated/untreated samples introduced to the system. Vacuum and pressure are supplied by two microdiaphragm pumps and actuated by an array of 32 solenoid valves.

The analysis layer, the “electrophoresis layer,” contains a μCE channel used for separations of processed samples into components differing in mass and charge. Sample introduction and separation is achieved across the channel via four tunable high-voltage electrodes powered by three miniature high voltage power supplies. As fluorescent dye-labeled analytes pass through the channel, they are excited by a 300 mW, 405 nm laser and detected by an Ocean Optics USB4000 UV-Vis spectrometer. Excitation and fluorescence emission are filtered by a series of bandpass and dichroic filters.

An Arduino Mega 2560 microcontroller is used to power and operate all electronic components in the instrument aside from the spectrometer. A tablet computer is used to interface with the spectrometer and microcontroller through software programmed in LabVIEW.

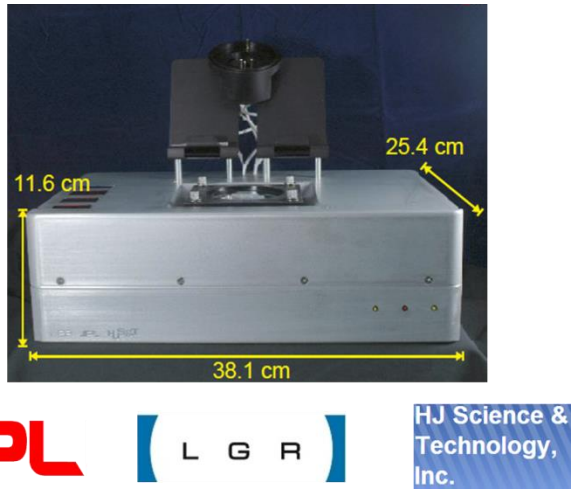

Figure 1: Assembled Chemical Laptop

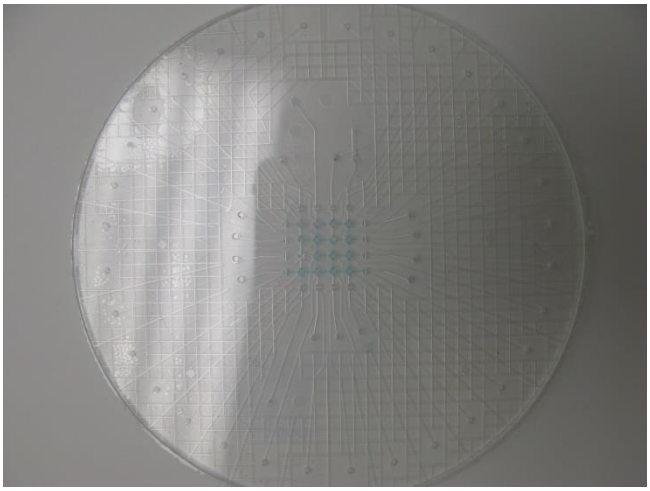

Figure 2: Multilayer microfluidic chip

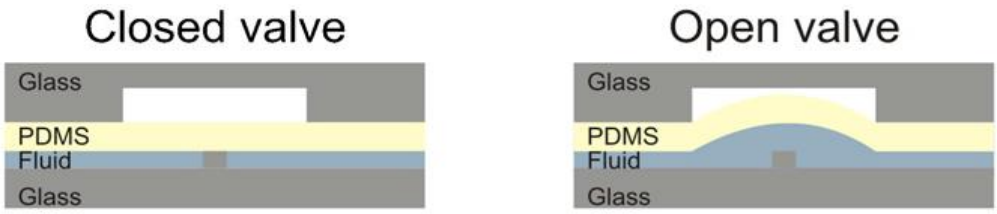

Figure 3: Cross-sectional representation of vacuum-induced valve actuation in our microdevices

III. Experiment

The primary objective of my work this summer has been to test and characterize the newly developed Chemical Laptop prototype, and prepare the instrument for a completely automated, end-to-end field analysis. This required modifications to existing hardware and software, and the development of new hardware and software. Here, these modifications and developments are described, as well as plans for the future.

A. Software Modification

Simplifying Spectral Data Output

The Chemical Laptop arrived at our laboratory with two LabVIEW programs developed by Los Gatos Research. The first program enables manual and automated control over the pneumatic system, high voltage electrodes, and laser. The second program allows real-time observation of the spectrometer’s measured signal across its entire wavelength range.

Since the LabVIEW program records the signal for 3648 different wavelengths every 50 ms, output files can become extremely large. For example, the output data for a 10 s measurement is a 3648 x 200 array. The size of these output files (5.7 MB for 15 s data collection) makes data analysis and file transfer inconvenient. Additionally, repeated measurements will take up a considerable amount of memory.

Two approaches were taken to reduce the file size of output data. First, modifications were made to the existing software to truncate the output data to a user-specified wavelength range. This was accomplished by altering and constructing several LabVIEW VIs. The pre-existing VIs used to control the Ocean Optics Spectrometer are designed to take in pixel number instead of wavelength. The spectrometer contains a CCD array with 3,648 pixels, each of which is mapped to a specific wavelength value by the following equation:

$$W(p) = 345.58 + 0.22p - 5.82 * 10^{-6}p^2 - 2.97 * 10^{-10}p^3 \qquad [1]$$

where W is wavelength (nm) and p is the pixel number. The first challenge was to create a VI which converted user-specified values of wavelength to their corresponding pixel number. The above equation 1 was graphed to create a mapping between every pixel number and its corresponding wavelength (Fig. 4). Regression analysis was then performed on the graph, yielding a 2nd order polynomial with R^2 of 0.999998:

$$W(p) = -7.4430641311 * 10^{-6}p^2 + 0.21746437067p + 344.8619612 \qquad [2]$$

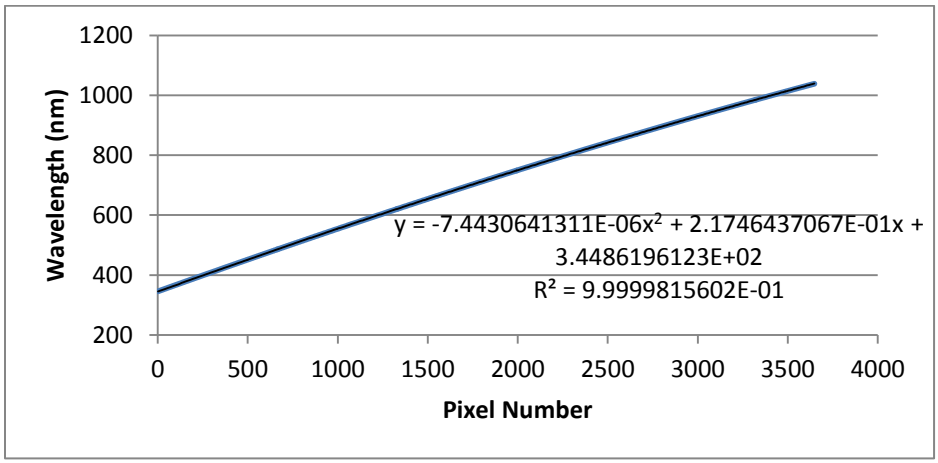

Figure 4: Relationship between wavelength and pixel number for the spectrometer by Eqn. 1

The VI, shown in Fig. 5, solves Eq. 2 using the quadratic formula and outputs the user-specified wavelength range in terms of pixel number.

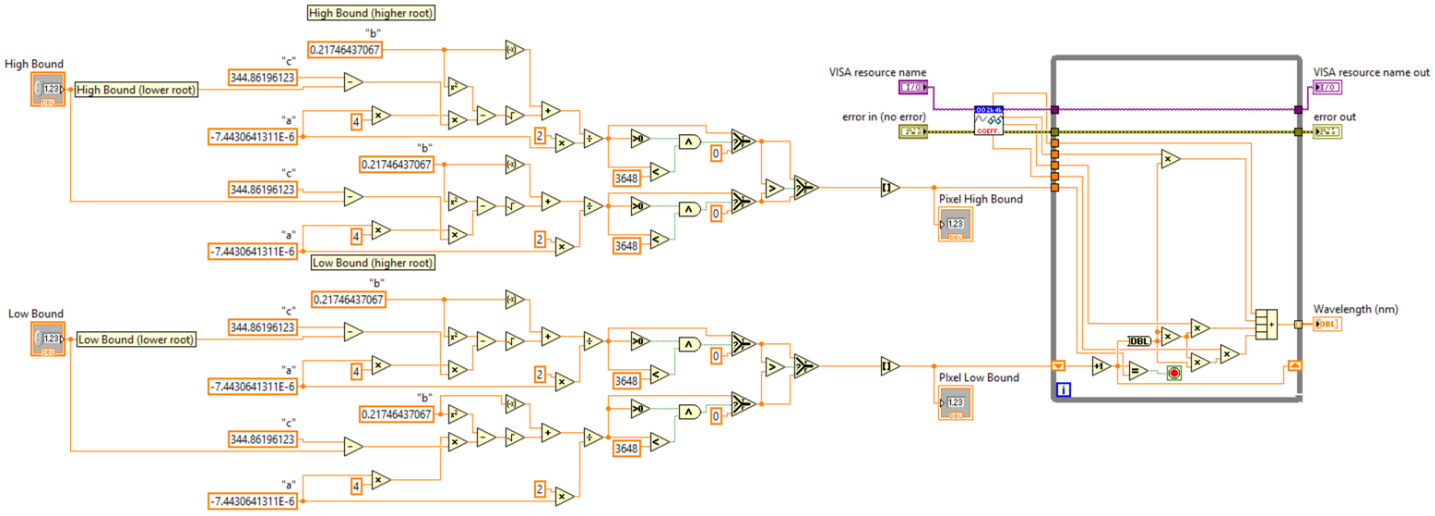

Figure 5: Wavelength to Pixel Converter VI. Converts user-specified wavelength range to pixel numbers by Eqns 1 and 2

Modifications were then made to the existing “readspectra” VI to read and record signal only within the specified range of pixel numbers. This was accomplished by adding functions which truncated the default output array of pixels to only those specified by the user via the Wavelength to Pixel Converter VI (Fig. 6).

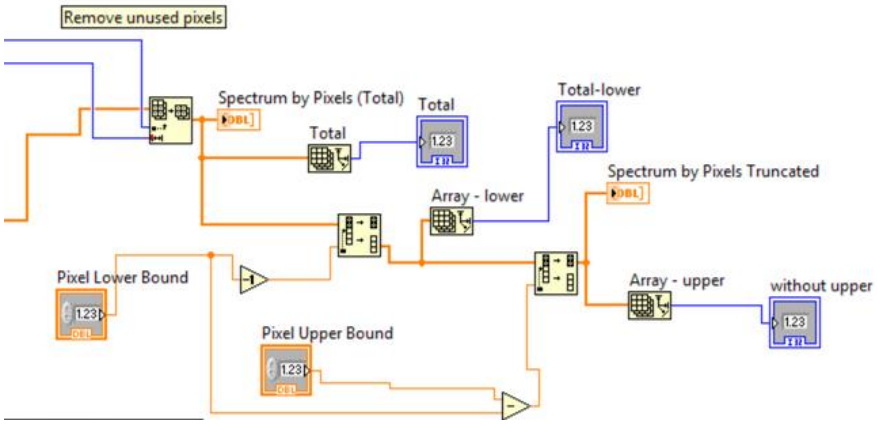

Figure 6: Modified read spectra VI containing functons to truncate the output array of pixels to the user-specified range

Secondly, to further reduce the size of output files, the existing LabVIEW observation program was modified to allow real-time observation of the integrated signal over the user-specified wavelength range. By consolidating the signal associated with every pixel into one averaged value, the output file could be reduced from a 2D array (wavelength vs. time vs. signal) to a two-column array (averaged signal vs. time). The interface for this program was designed to allow the user to save the original array file, the averaged signal two-column array file, or both (Fig. 7).

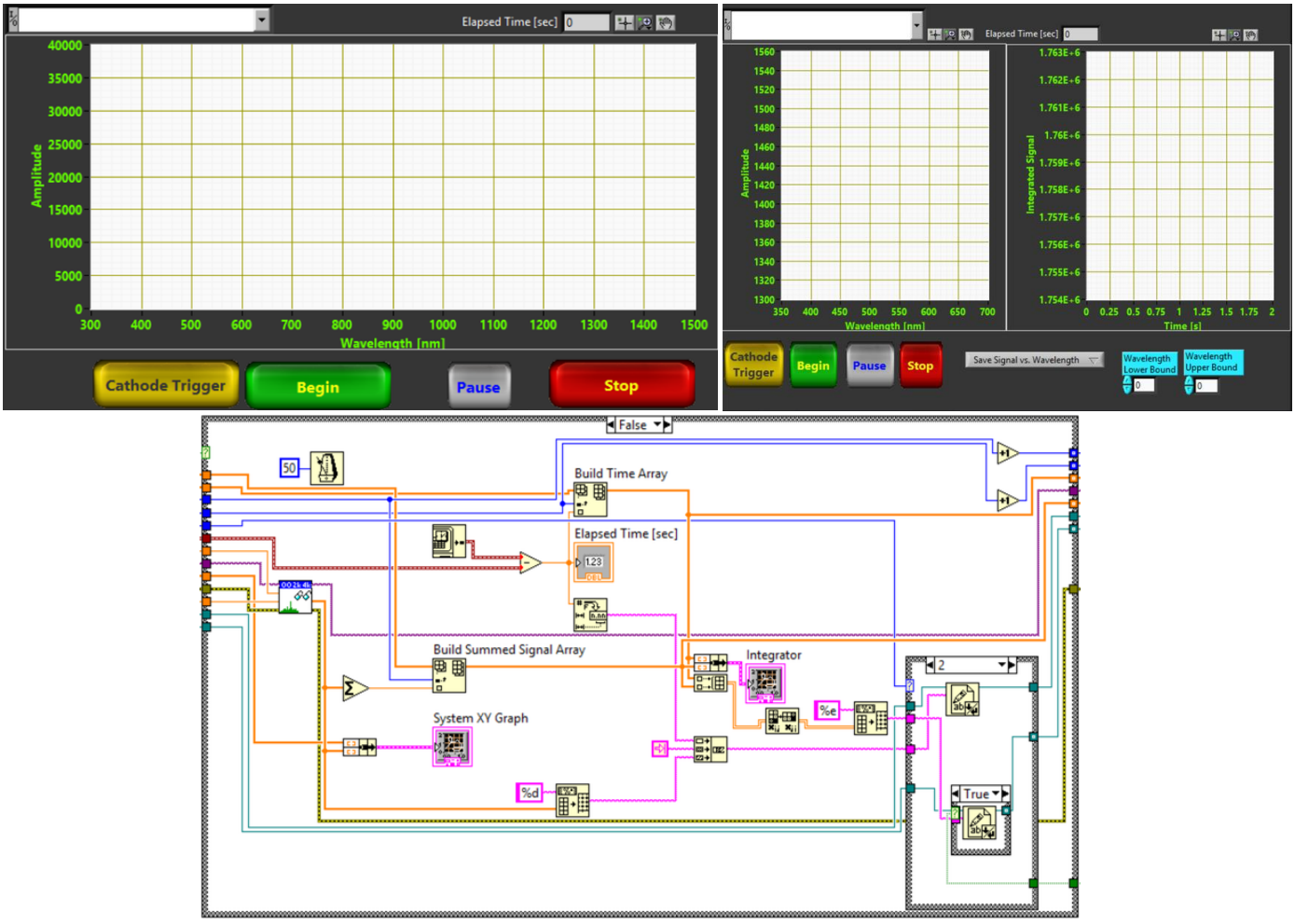

Figure 7: New interface and block diagram (top left and bottom), and old interface (top right) for the spectrometer observation program.

Optimization of Existing Labeling Protocols

Since our microfluidic chips are manually assembled, each chip differs in certain qualities like fluidic resistance. Whenever a new chip is assembled, the optimum wait time between valve actuations must be characterized. At long waiting times between valve actuations, the valves open and close completely, and therefore shorter waiting times results in faster fluidic transfer. At short waiting times, the membrane has inadequate time to fully deflect, and therefore does not open or close completely, leading in a reduction in the amount of fluid transferred per pumping iteration and thus slower fluidic transfer. Therefore, a careful optimization was required to determine the optimal waiting time to balance these contradictory effects.

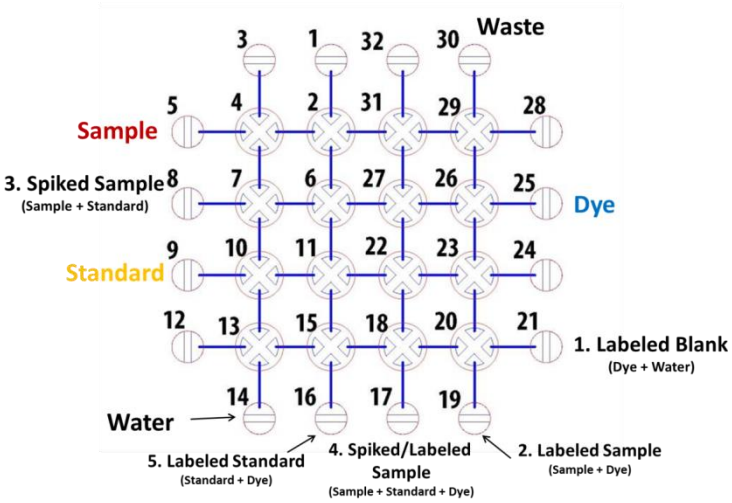

Fig. 8: Amino Acid Analysis pumping protocol. Numbers indicate chronological order of mixing

Experiments were performed with the amino acid analysis pumping protocol (Fig. 8) using food coloring representative of sample, standard, and dye labels. The volume recovered from storage reservoirs after each mixing cycle was measured three times successively for wait times of 100, 200, 300, 400, and 500 ms. Averaged values and their error bars were plotted for each wait time (Fig. 9). Additionally, the difference in fluid volume between the “labeled spiked sample” and “spiked sample” reservoirs was determined as a rough measure of fluidic transfer between reservoirs (Fig. 10). The highest volume recovered from storage reservoirs after analysis was noted at 400 ms; however, these values show a certain amount of inconsistency. With a wait time of 500 ms, similar volumes (albeit slightly lower) were recorded with a much greater consistency across reservoirs and trial runs. Additionally a greater consistency in measurements of fluidic transfer from the “spiked sample” reservoir to the “labeled spiked sample” reservoir was noted with a 500 ms wait time.

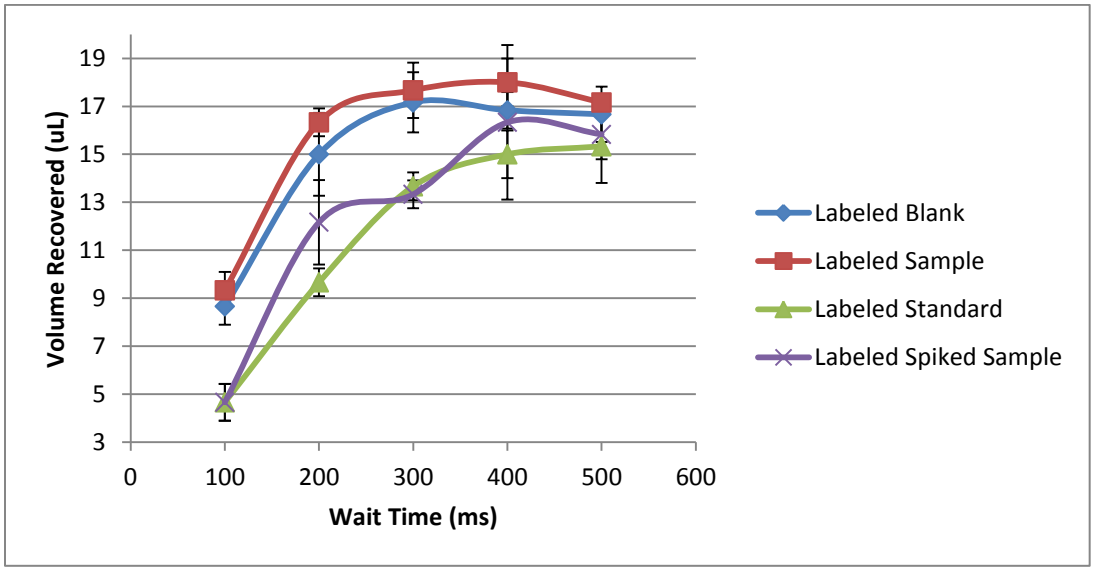

Fig. 9: Reservoir volumes vs. wait time for Amino Acid Analysis pumping protocol

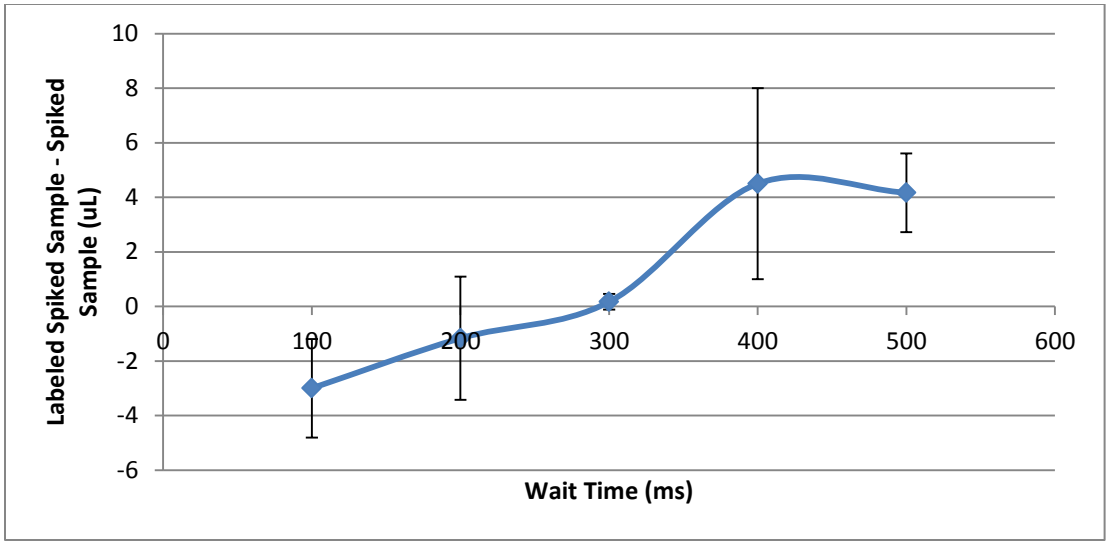

Fig. 10: Volume differential between wells 4 and 3 vs. time for Amino Acid Analysis pumping protocol

B. Software Development

Optimization of Rinse Cycles

The wash cycle in the transcribed OCW programs involve a filling step where all valves in the pneumatic chip are filled with water from the water input reservoir and an emptying step where all valves in the chip are sequentially closed from the water input reservoir to the waste output reservoir, ejecting all fluid to waste. This wash cycle is repeated 5 times with a wait time of 200 ms. For certain steps in the amino acid analysis pumping protocol, this wash cycle did not adequately rinse the pneumatic chip. To correct this issue, many alternative washing cycles were explored. Four methods were examined with wait times of 100 ms and 200 ms. For each of these eight methods, elapsed time, total volume consumed, and total number of valve actuations were recorded. These values were plotted in a bubble graph (Fig. 11), with process time and valve actuation plotted on the x-y axis, and total volume consumed represented by the diameter of each bubble.

While testing additional rinse cycles, I noticed that liquid was leaking into one of the dye reservoirs during each iteration. After further testing, I found that this occurred during each of the eight methods recently developed – namely, when the entire volume of liquid in the fluidic layer is pushed to the waste reservoir. A bottleneck effect occurs at this point, which is connected to the valve array by only one channel. The fluidic pressure at this point was high enough to overcome the closing pressure of adjacent reservoir valves, and force fluid through.

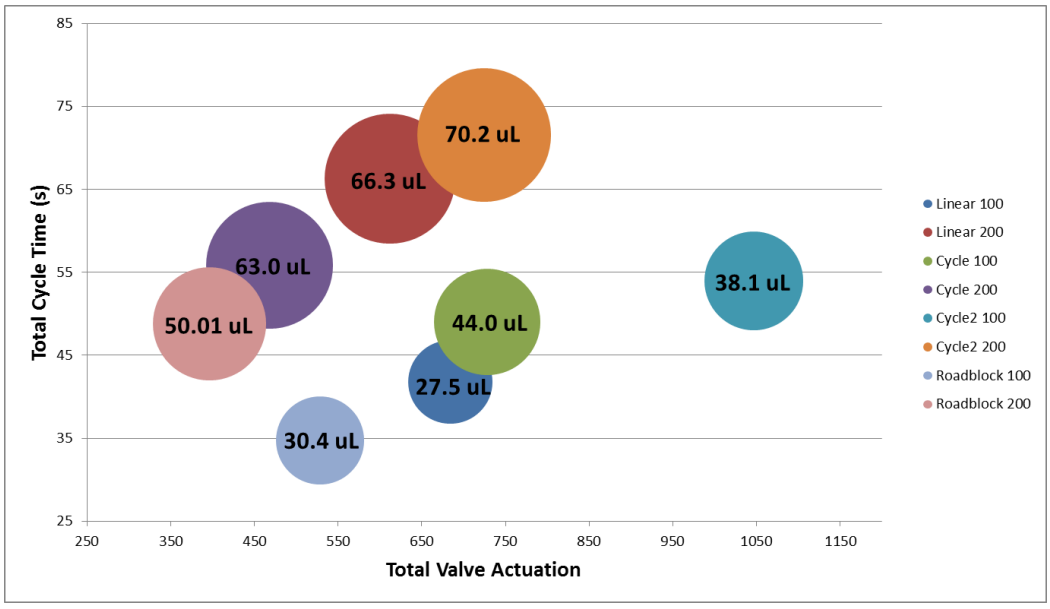

Fig. 11: Comparison of optimization factors for rinsing cycles

To resolve the issue, modified rinse cycles were developed using smaller input volumes of water to reduce the bottleneck effect during waste export. These cycles are outlined in Fig. 12. Like before, time elapsed, volume consumed, and number of valves actuated were recorded and graphed (Fig. 13). REPoly was chosen as the optimum method. Though it consumes the greatest volume, it consumes the least amount of power (868 valve actuations) and has a relatively low process time of 57.75 s. Additionally, as seen in Fig. 14, REPoly has the fastest rate of rinsing compared to other methods. Since realistically, our samples will be far less concentrated than the dyes used in these experiments, the rate of rinsing is perhaps the most important factor in determining an optimum method.

C4E100 (W = 100)

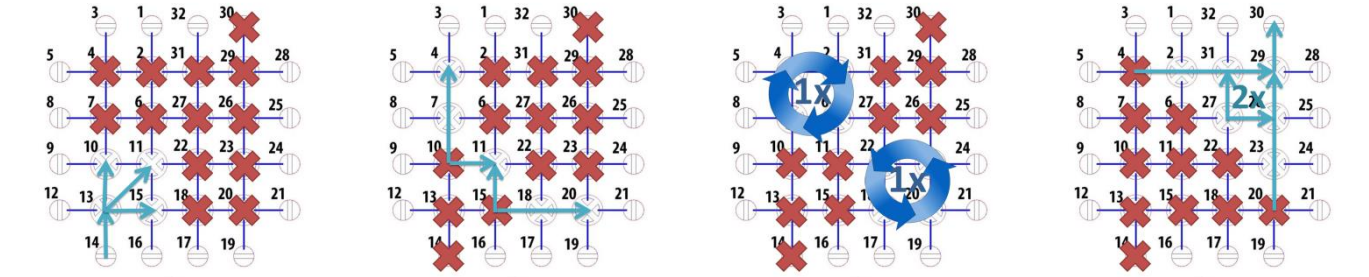

LE100 (W = 100) and **LE200** (W = 200**)**

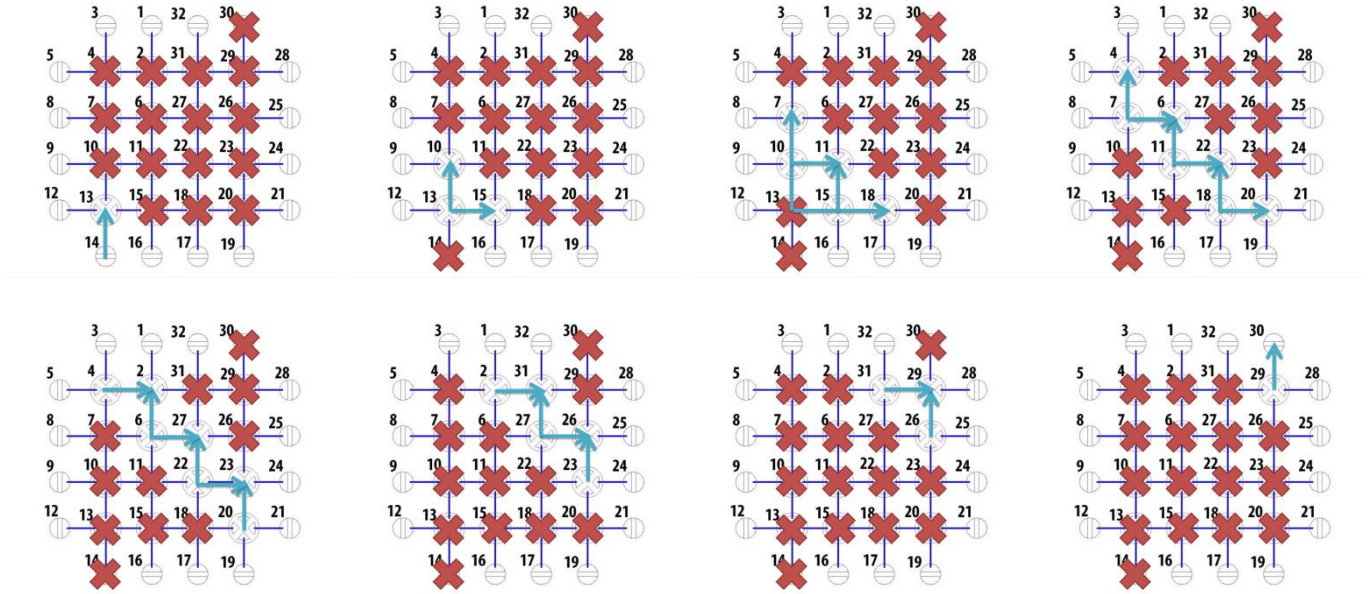

REPoly (W1 = 100, W2 = 200)

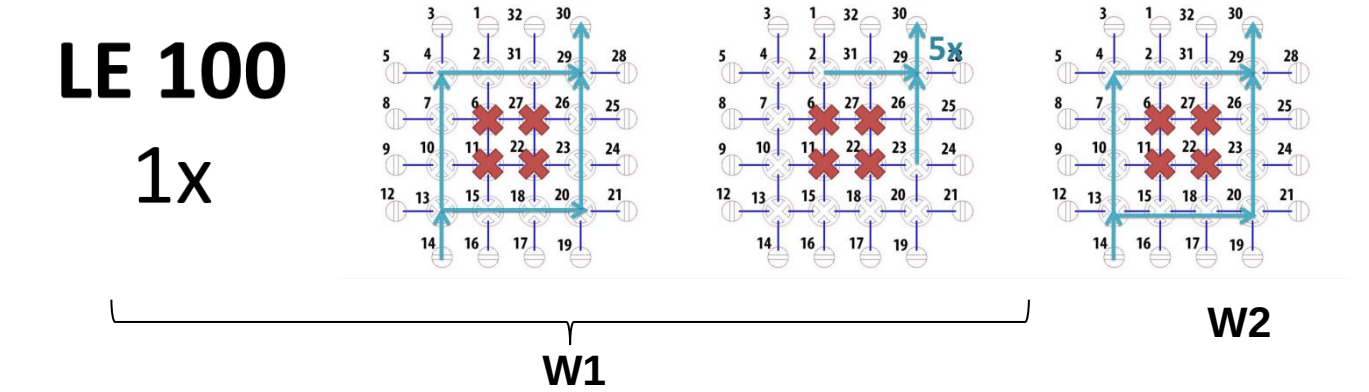

Fig. 12: Finalized low volume, low pressure washing cycles

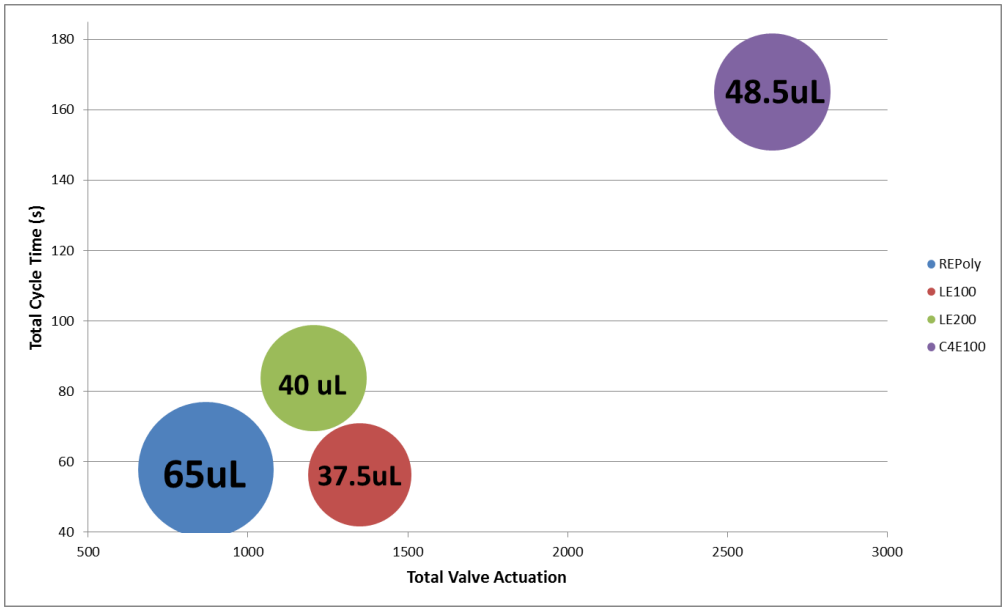

Fig. 13: Comparison of optimization factors for low volume, low pressure wash cycles

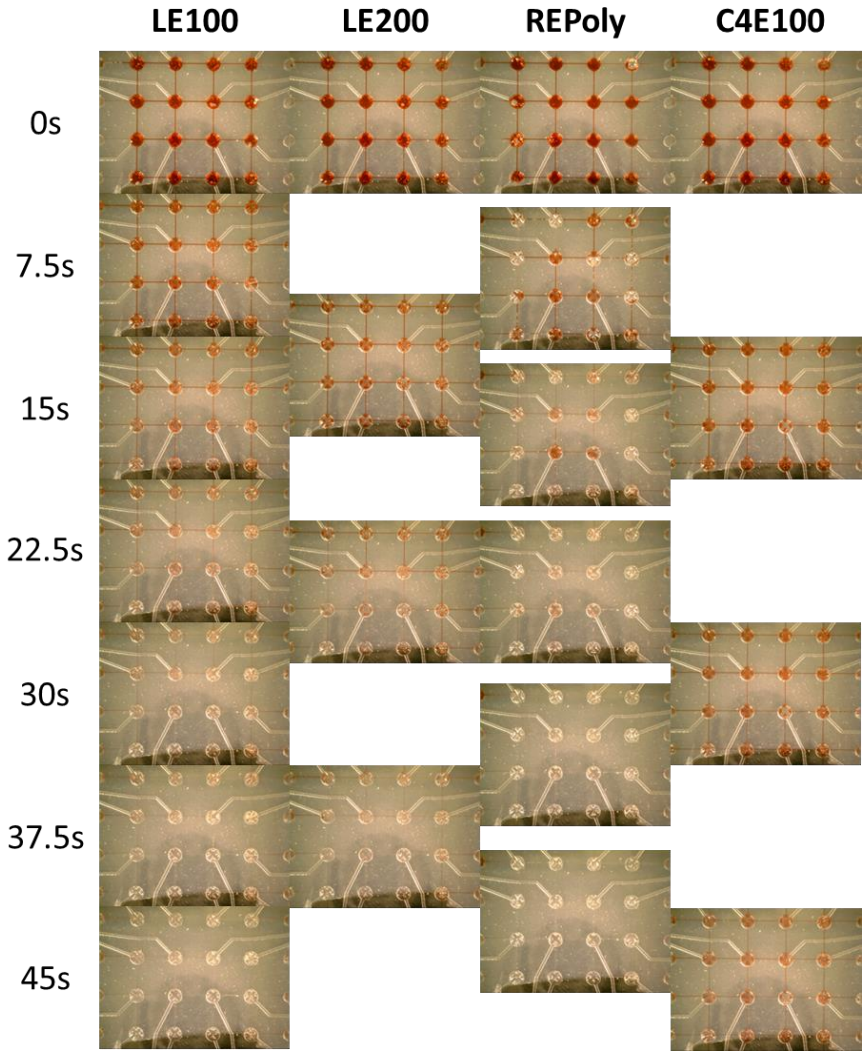

Fig. 14: Pneumatic layer after consecutive rinses for each wash cycle

Digital Colorimetric pH Tuning

The Willis Group has succeeded in labeling and detecting amino acids, carboxylic acids, aldehydes, ketones, thiols, and polycyclic aromatic hydrocarbons using µCE-LIFD. The labeling reactions for each of these compound classes are pH specific. Amino acids label at pH 9, carboxylic acids label at pH 3, and so on. An automated method for adjusting the pH of a field sample is thus desirable. To accomplish this, two things are necessary: the ability to measure pH and the ability to adjust it to a specified value. With our processing chip, pH adjustment is trivial. One simply has to program an automated cycle to mix the sample with a small volume of base or acid stored in one of the processor's reservoirs. Measuring the pH of the sample after each addition is a little trickier. Standard methods for measuring pH show little practicality for the Chemical Laptop. Microelectrodes are small enough to fit in the reservoirs of the processing chip, but require careful handling, periodic calibration, maintenance (reference solution must be replaced every so often), and thorough cleaning before storage. In addition, these electrodes require circuits/adapters to translate measured potentials into digital signals which could be sent to our LabVIEW control interface. Such circuitry exists, but requires calibration, additional power supplies, and money. To achieve a truly automated analysis with the Chemical Laptop, an alternative way was needed to measure pH.

Digital Color Representation as a Measure of pH

Experiments were performed to explore the possibility of using the digital color representation of an imaged, indicator solution as a measure of pH. It was imagined that by quantifying the RGB (red green blue) profile of an indicator solution at several points during it's color transition, an RGB threshold value could be determined which marked the end of an indicator's transition.

First, software was developed to measure the average RGB color composition of a region of interest (ROI) in a digital image. Pictures were taken of three indicator solutions using a Dinolite USB Microscope, after several successive 0.5 µL additions of 5 mM NaOH. The RGB profiles for each indicator were then measured and plotted as a function of base addition (Fig. 15). For all three indicators, the R and G values showed significant change during color transition, and a clear RGB threshold profile marking the end of color transition. These results showed that it was entirely feasible to develop a colorimetric method for automated pH adjustment based on digital color representation.

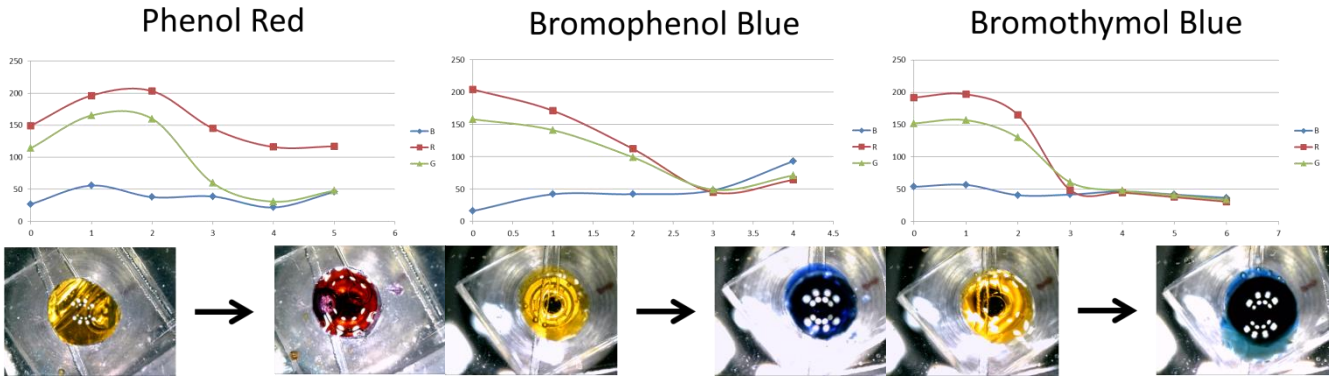

Figure 15: Changes in RGB profile associated with the color transition of three indicators

Developing Software for Automated, Digital Colorimetric pH Tuning

New software was then developed which could: 1) measure the average RGB profile of an indicator solution as displayed by a mounted USB microscope, 2) automatically add base/acid to the solution until a desired color transition had been achieved (as determined by an RGB threshold), and 3) automatically label the pH-adjusted sample, along with a blank, standard, and spiked sample, for analysis by µCE-LIFD. The interface for this program (Fig. 16) displays a real-time video stream from the USB microscope. Sliders on the right and bottom of this display allow the user to crop displayed images to a specified ROI. The average RGB values of this cropped region are then displayed on the interface. Status and process indicators on the display the current cycles and pumping routines being performed on the processing chip.

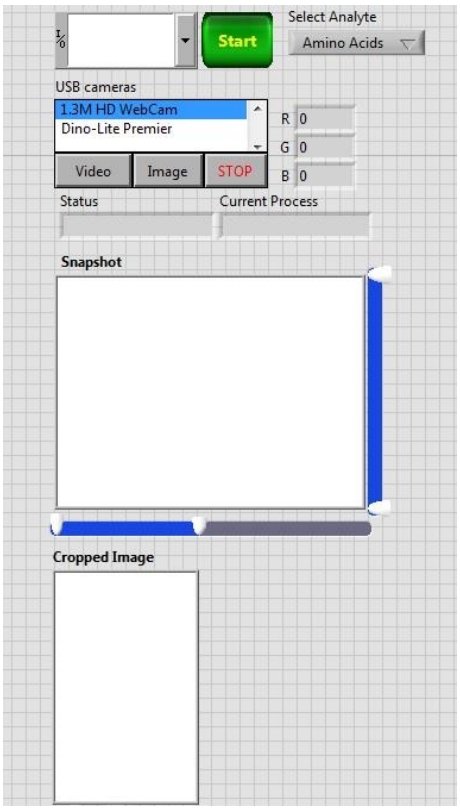

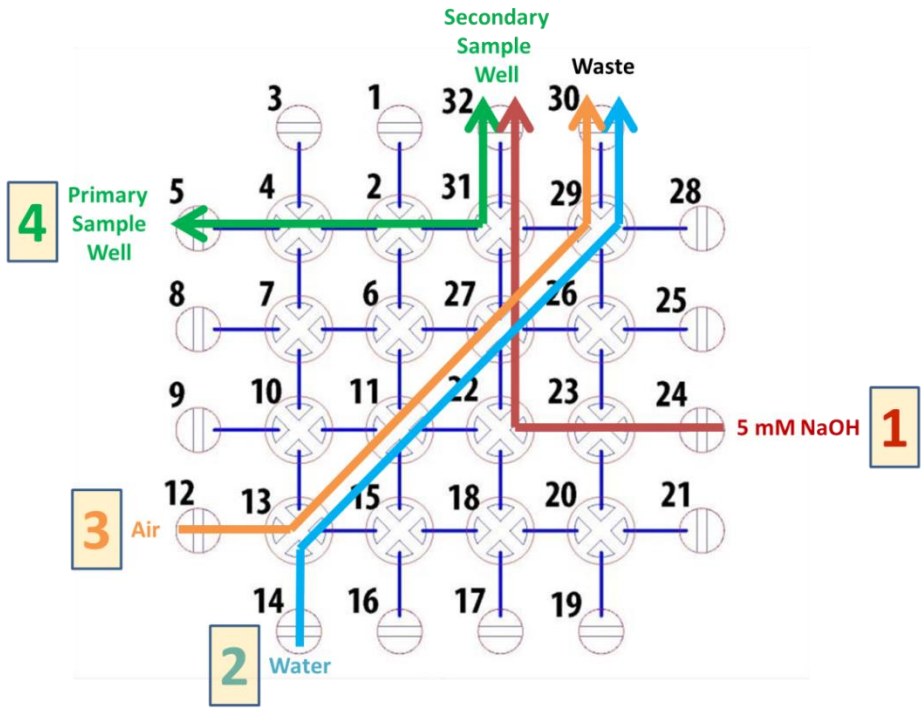

Figure 16: (Left) Interface for automated colorimetric pH adjustment and labeling software.
Figure 17: (Right) Outline of the pH adjustment routine with numbers indicating chronological order of processes

The program, written in LabVIEW, uses National Instruments IMAQ drivers to interface to the USB microscope. The program takes each frame captured by the microscope and breaks it down into individual pixels. Each pixel is then assigned an 8-bit integer (0 - 255) corresponding to R, G, and B. The average values for R, G, and B within the specified ROI are then averaged and displayed. When the user decides to begin automated pH adjustment and presses “Start,” a snapshot is taken, and the RGB values of that snapshot are compared to experimentally determined threshold values for the indicator. If the threshold has not yet been reached, the process outlined in Figure 17 is initiated. First, base (or acid) is added to a secondary sample well. Then, the processor is rinsed with water and dried with air. The sample solution (with indicator) is then “mixed” by transferring it from the primary sample well to the secondary well and back to the primary well. Once the process completes, another snapshot is taken of the solution in the primary well, and RGB values of this snapshot are again compared to the threshold. These steps are repeated until the threshold is reached. Once reached, a “verification” step is initiated where the sample is transferred to the secondary well and back. This is to ensure complete mixing. If the RGB values are still past the threshold, automated labeling routines are performed with the pH-adjusted sample.

µCE – LIFD Analysis of a pH – Tuned Sample

For our analyses, amino acids must be labeled at pH 9 with fluorescent pacific blue dye. Phenol red, which turns from yellow to red at pH 8.2, was thus chosen as the pH indicator for amino acid analyses. Since later labeling steps involve the use of a pH 9 borate buffer, a sample pH of 8.2 is effectively close enough to pH 9 to achieve labeling of pacific blue. Before using phenol red, a proper threshold RGB profile had to be experimentally determined. Using the process outlined in Figure 4 with no specified threshold, successive base additions to 1 mM solution of phenol red were performed. Experiments were performed using four types of “mixing” cycles varying in the amount of fluid transferred between the primary and secondary wells. The results are outlined in Figure 18. In this figure, the red box is used to indicate the trial at which the solution appeared satisfactorily red. In all cases, R and G values showed significant change, while B values remained constant. Out of all four mixing cycles, the 30/25 rep mixing cycle showed the sharpest, clearest decrease in R and G values. This cycle was further examined to determine a proper threshold. Three additional trials were performed where R and G values were recorded before base addition to the indicator and at the point where the indicator was satisfactorily red, along with the number of iterations required to reach that point. The results, outlined in Table 1, show that phenol red’s color transition from yellow to red is generally marked by a R value less than 150 and G value less than 30.

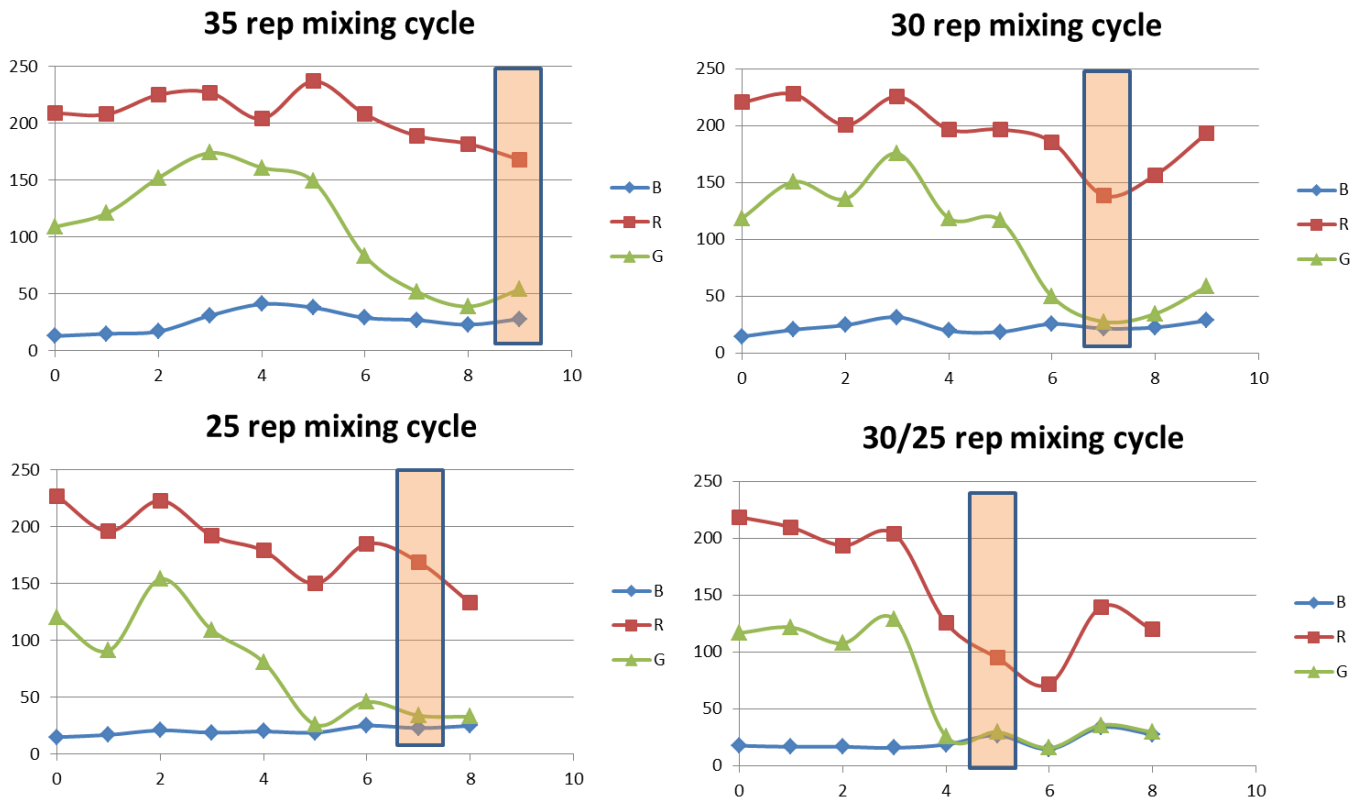

Figure 18: RGB profiles of phenol red during color transition for four mixing cycles varying in sample volume transferred per iteration

	Initial State		After Titration				
Trial	R	G	R	G	ΔR	ΔG	iterations required
0	227	120	95	30	132	90	5
1	219	117	125	23	94	94	8
2	192	114	57	19	135	95	10
3	207	112	132	17	75	95	4

Table 1: Initial and final R and G values for 4 trials performed with the 30/25 repetition mixing cycle

Using these threshold values, the software was tested on a mock amino acid sample containing 1 mM phenol red. Experiments were performed in triplicate. An outline for the completed automated procedure is shown in Figure 19**.** As emphasized in the figure, aside from selecting a ROI and target analyte, every step in this procedure is completely automated. Since a CE chip for the Chemical Laptop had not yet been fabricated, analysis of the pH-adjusted samples was performed on another system in the lab. The results, shown in Figure 20, show consistent measurements for blank, sample, and standard solutions across all three trials. Additionally, peak area and amplitude of all amino acids in the mock sample show great consistency across runs. These results demonstrate the success of the process shown in Figure 20 and the software used to implement it.

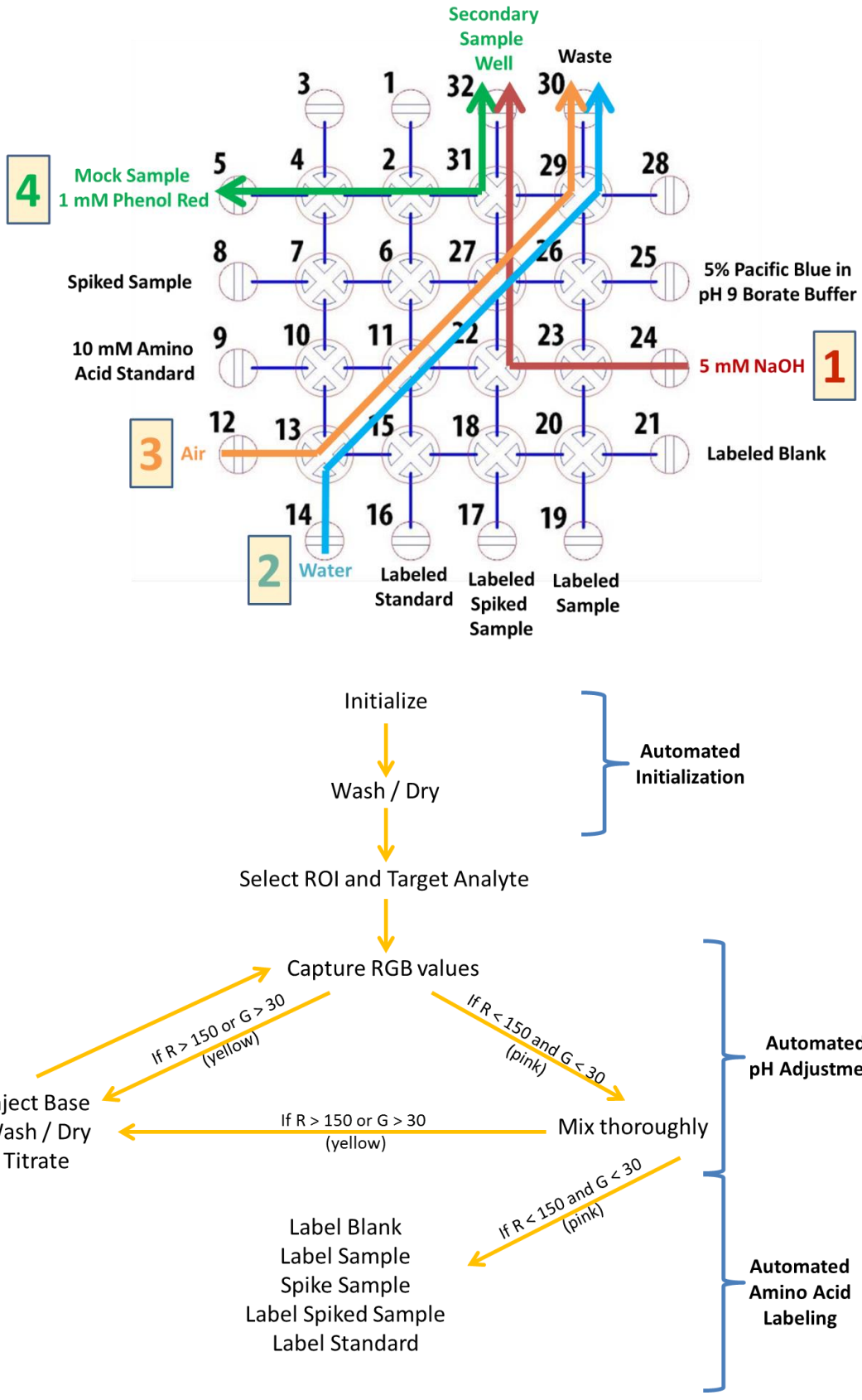

Figure 19: (Top) Reservoir assignments for reagents used during automated pH adjustment and labeling of amino acids. (Bottom) A flow chart outlining the process of the automated routine

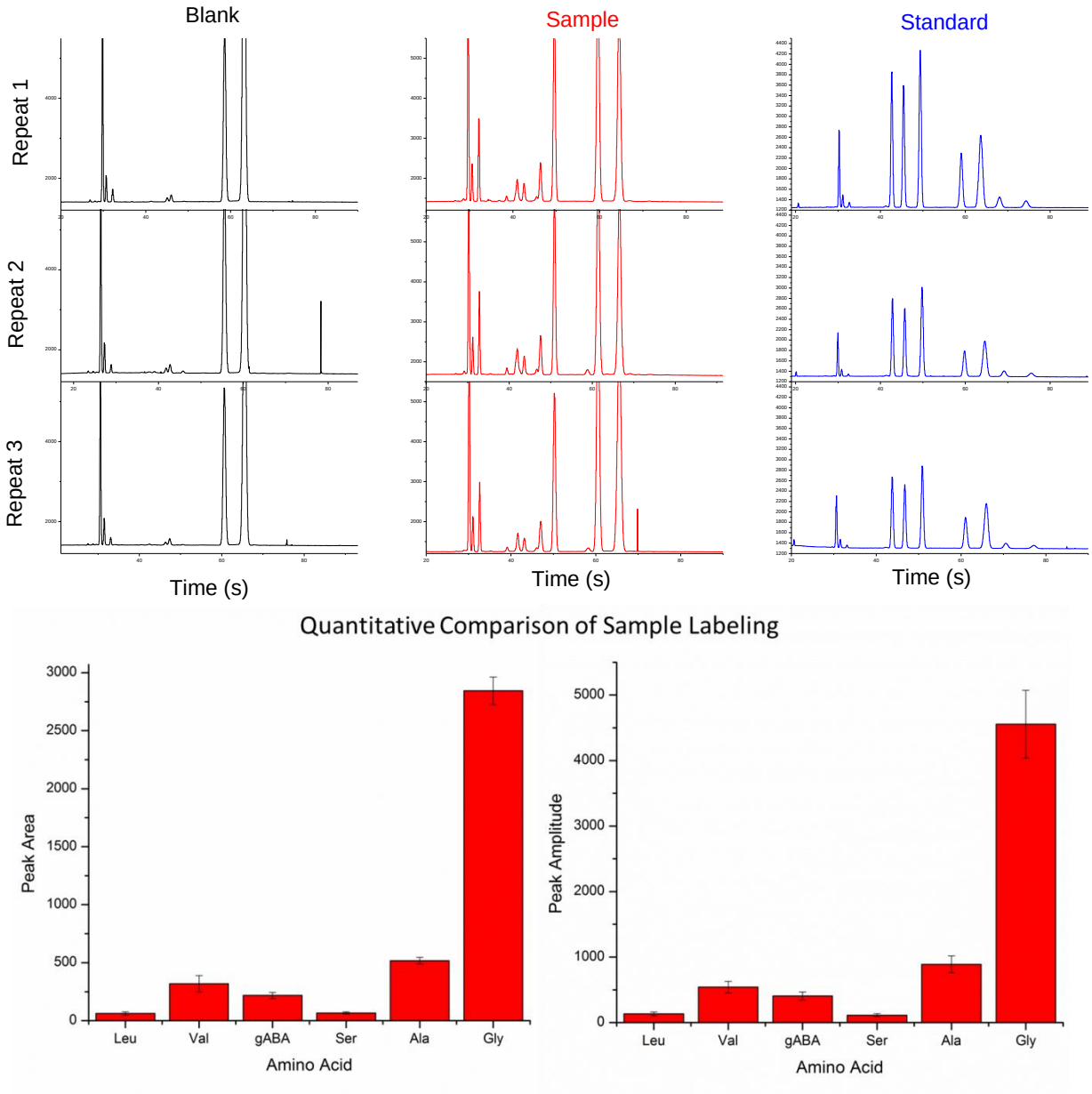

Figure 20: (Top) Electropherograms of solutions generated by the automated pH adjustment and labeling routine. (Bottom) Peak areas and peak heights for amino acids detected in the mock sample.

Hardware Modification:

Experiments were performed to expand the colorimetric pH tuning software towards carboxylic acid and thiol analysis. However, hardware issues appeared, namely, leaking and sticking valves. Previously, these hardware issues could be bandaged with careful, clever programming (i.e. redesigned rinse cycles to prevent leaking during waste export cycles); but when programming more complex sequences (like automated pH adjustment), these issues could not be fixed as easily. Changes to the hardware were necessary before further experiments were performed.

Upgrading Microdiaphragm Pumps

It was thought that leaking issues were partly due to the insufficiency of the Chemical Laptop's pressure pump (TCS D200S). The pump (400 mBar operating pressure) might not have been supplying enough pressure to keep the PDMS valves in the processor closed. To confirm this notion, experiment were performed substituting nitrogen gas at 750 mBar as the pressure source. With this higher pressure actuating the valves closed, there was absolutely no leaking through the valves on the outer rim of the processor – even with high speed, high volume rinse cycles. However, leaking throughout the center valves was still apparent. In light of these results, a stronger pressure pump (Parker-Hannifin #124-11) with an operating pressure of 24 psi was purchased and installed.

Redesigning Pneumatic Manifold

It was also speculated that our issues may have been caused by a warped pneumatic manifold. The pneumatic manifold (Fig. 21) is an essential part in the instrument, serving as the interface between the microfluidic chip and the pressure and vacuum sources. As shown in the figure, the microfluidic chip is clamped atop the manifold. The interfacial surface between the manifold and the chip must be completely flat, even with a gasket, to ensure that there is an even distribution of weight on the chip, and no leaking of pressurized air. The part is very complex, containing a series of internal channels and sharp corners, making it impossible to machine in just one piece. The part was thus 3D printed by a ProJet machine in a material called EX200. With any 3D printing process, a waxy support material is used to fill any empty space in the design, so that the piece does not collapse upon itself during printing. With ProJet Machines, the support material is easily removed by heating the part in isopropyl alcohol. Unfortunately, this process also warps the piece to a degree non-trivial for our purposes. In an attempt to “unwarp” our EX200 manifold, the manifold was clamped down in an oven at 65 °C for 2 hours and subsequently placed in a freezer at -20 °C overnight. The manifold was then reinstalled in the instrument and tested. Initially, all leaking issues appeared to be fixed. Though, a couple hours later, the manifold rewarped and the issues resurfaced. It seemed that EX200 might not be a sufficient material for our purposes.

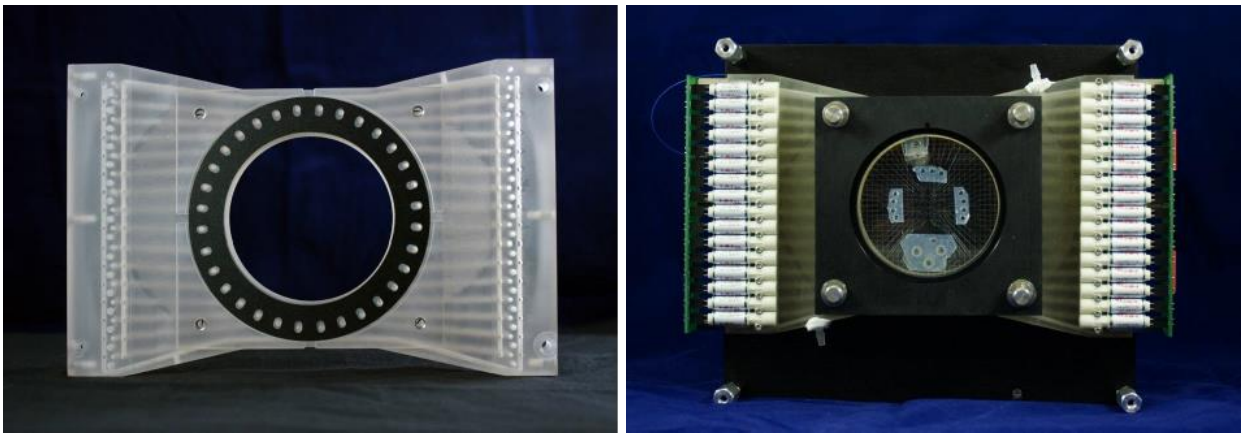

Figure 21: (Left) Unassembled EX200 pneumatic manifold. (Right) Assembled EX200 pneumatic manifold with solenoid valves mounted on either end, and a polycarbonate clamp mounted on top to hold the microfluidic chip in place

An alternative 3D printing process, PolyJet, was explored for the pneumatic manifold. The PolyJet material, VeroWhite, machine, was chosen because it was non-porous and structurally stable. Additionally, PolyJet process uses a water-soluble support material typically washed away with a pressurized water stream – there is no heat involved. However, the support material was very difficult to remove from the manifold’s thin, sharply angled internal channels. Several techniques were explored to remove the support material, with little success. The part was then redesigned to make the support material easier to remove (Figure 22). This design included several intercepting channels allowing a thin metal rod to be inserted inside to scrape out the support material. This made removal of the support material much easier. After removing the support material, threaded inserts and plugs were installed to mount the 32 solenoid valves and clamp. The manifold was then installed and tested. During testing, leaking was discovered at the interface between the manifold and the solenoid valves. This material may work as an alternative, if all mounting interfaces are milled completely flat post-fabrication. More work will need to be done to confirm this notion.

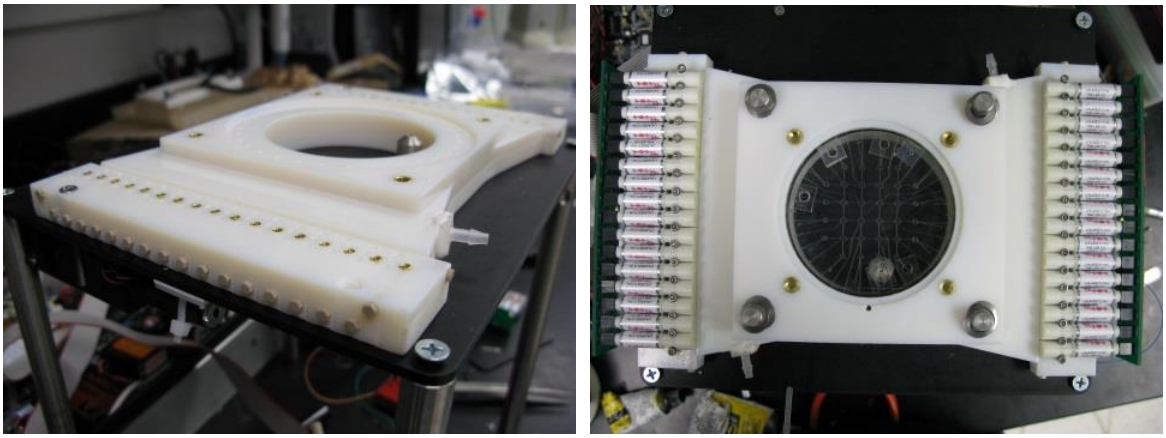

Figure 22: Redesigned VeroWhite pneumatic manifold unassembled (left) and assembled (right)

Another alternative for fabricating the pneumatic manifold was to mill it out of aluminum in three separate layers, and then clamp the layers together with silicon rubber gaskets in between. Though this method is more expensive, it would certainly result in a flat mounting interface for the microfluidic chip and solenoid valves. The redesigned, three-layer pneumatic manifold was sent to FirstCut to be machined, and customized gaskets were designed and sent to the Tulsa FabLab to be laser-cut out of silicon rubber (Fig. 23).

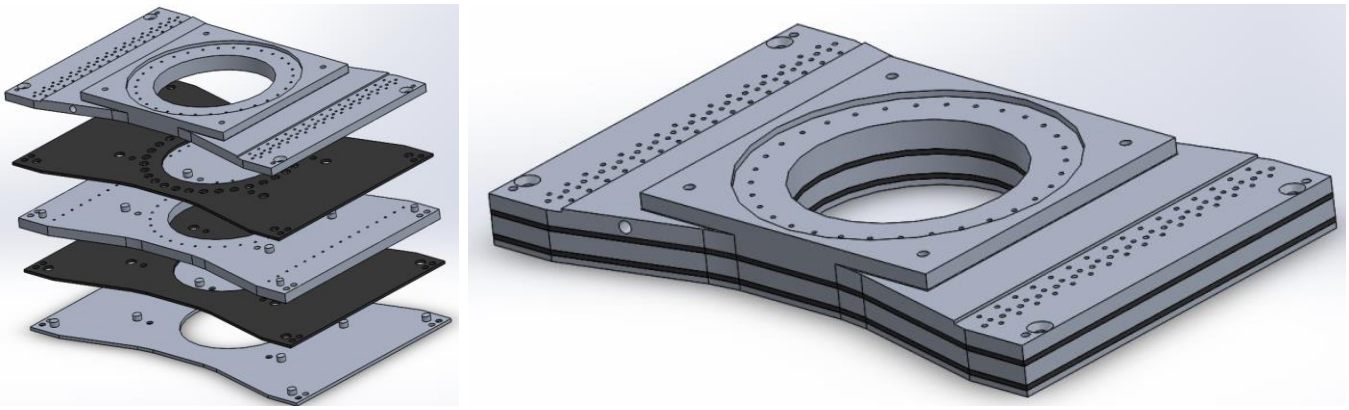

Figure 23: Solidworks design for three-layer aluminum manifold with silicon gaskets

Redesigning Manifold Clamp

Lastly, it was speculated that leaking issues may have partly been caused by the pneumatic manifold's clamp. When the instrument was disassembled, it became apparent that when the chip was fully clamped down to the manifold, the existing polycarbonate clamp was warping significantly around the corners where the mounting screws were attached. This warping was a likely explanation for our leaking issues. Since most of the weight is distributed about the corners, it makes sense that adequate pressure was being supplied to outer valves, but not inner valves. The same clamp design was sent to FirstCut to be milled out of aluminum. With a stiff aluminum clamp, force would be evenly distributed about the top of the chip when fully clamped.

Hardware Development

Exchangeable Reagent Cartridges

Currently, the reagents for our analyses must be manually deposited on the surface of the microfluidic chip, in PDMS reservoirs capable of holding no more than 60 µL of liquid. Since different types of analyses require a different set of reagents, the PDMS reservoirs must be emptied and rinsed manually between different analytical formats. This works, but a more automated method for dispensing reagents would be preferrable.

I began prototyping miniature, refillable, exchangeable, reagent "cartridges" designed to dispense all necessary reagents required for the analysis of numerous compound classes by a simple clamping and switching mechanism. It was envisioned that before field analysis, one could prepare a set of reagent cartridges, each containing all the reagents necessary for analysis of a particular functional group, and perform all analyses back-to-back by simply installing new cartridges atop the instrument.

The first prototype cartridge was 3D printed in VeroClear material with a PolyJet machine (Fig. 24). It contains 12 reagent reservoirs, each capable of storing more than 300 µL, and four holes for the electrodes necessary for electrophoresis. A partially overmolded, VeroClear rotating disc is placed inside the cartridge. This disc is designed so that when rotated to the "closed" position, it creates a physical barrier between the reagent's stored above, and the microfluidic chip mounted below. When the disc is rotated to the "open" state, the reservoirs are no longer obstructed, allowing reagents to drop down onto the surface of the chip. A rubber gasket attached on the bottom cartridge is designed to create a tight seal to the chip when clamped down by four mounting screws at the corners. The design shown in Figure 24 has not yet been finalized. Updates need to be made to prevent leaking between reservoirs at the interface of the internal switching disc. A rotor-stator mechanism is currently being conceived.

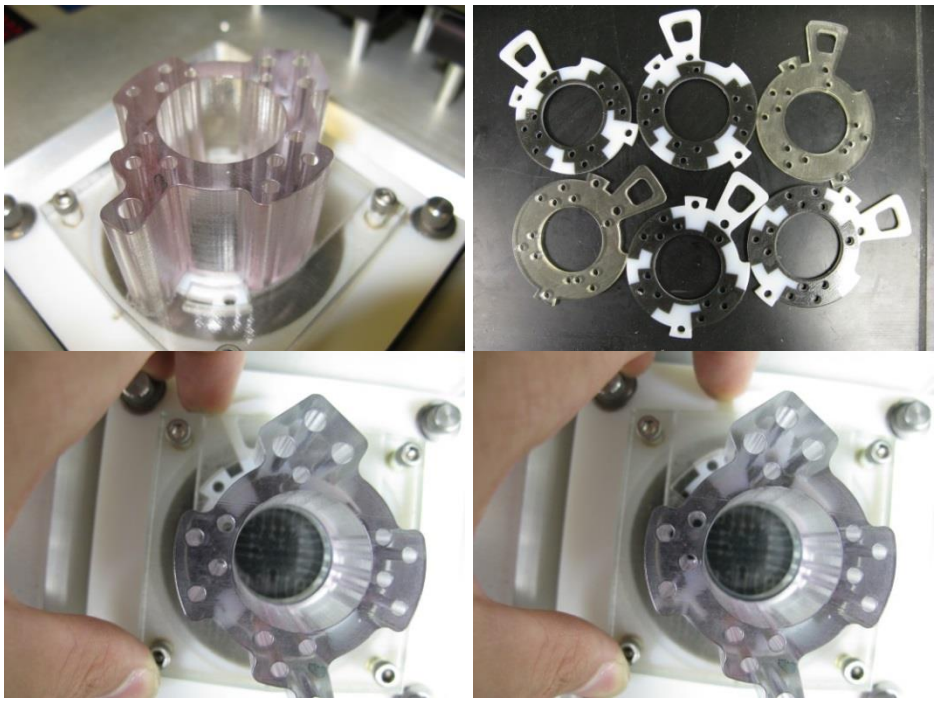

Figure 24: Prototype design for exchangeable reagent cartridges. (From top to bottom) Cartridge mounted atop the instrument, internal rotating discs, cartridge in “closed” switch state, and cartridge in “open” switch state.

Future Work

Once the aforementioned hardware issues are resolved, it will be possible to test the instrument’s detection system, and characterize detection limits for each of our labeling processes. The instrument will then be ready for field testing. While the design of exchangeable reagent cartridges would be convenient, it is not absolutely necessary for field analysis.

IV. References

[1] P. A. Auroux, D. Iossifidis, D. R. Reyes and A. Manz, “Micro total analysis systems. 2. Analytical standard operations and applications”, Anal. Chem., 2002, 74, 2637-2652.

[2] D. R. Reyes, D. Iossifidis, P. A. Auroux and A. Manz, “Micro total analysis systems. 1. Introduction, theory, and technology”, Anal. Chem., 2002, 74, 2623-2636.

[3] C. Berg, D. C. Valdez, P. Bergeron, M. F. Mora, C. D. Garcia and A. Ayon, “Lab-on-a-robot: Integrated microchip CE, power supply, electrochemical detector, wireless unit, and mobile platform”, Electrophoresis, 2008, 29, 4914-4921.

[4] D. J. Jackson, J. F. Naber, T. J. Roussel, Jr., M. M. Crain, K. M. Walsh, R. S. Keynton and R. P. Baldwin, "Portable High Voltage Power Supply and Electrochemical Detection Circuits for Microchip Capillary Electrophoresis," Anal. Chem., 2003, 75, 3311-3317.

[5] Clifton, M.J., Roux-de Balmann, H., Sanchez, V., “Protein separation by continuous-flow electrophoresis in microgravity”, AiChe. J., 42 (70), 2069-2079, (1996).

V. Acknowledgements

This research was carried out at the Jet Propulsion Laboratory, California Institute of Technology, and was sponsored by the Summer Undergraduate Research Fellowship program and the National Aeronautics and Space Administration. We thank Los Gatos Research and HJ Science & Technology for their assistance in engineering the Chemical Laptop, and Michael Armbruster at Incept 3D for his help with 3D printing processes and materials.